

Gamow-Teller strength in the $^{26}\text{Mg}(\text{p},\text{n})^{26}\text{Al}$ reaction at 135 MeV and its fractionation into $T=0, 1$, and 2 isospin channels

R. Madey, B. S. Flanders,* B. D. Anderson, A. R. Baldwin, C. Lebo, and J. W. Watson
Department of Physics, Kent State University, Kent, Ohio 44242

Sam M. Austin, A. Galonsky, and B. H. Wildenthal†
Department of Physics and Astronomy and Cyclotron Laboratory, Michigan State University, East Lansing, Michigan 48824

C. C. Foster
Indiana University Cyclotron Facility, Bloomington, Indiana 47405
 (Received 6 March 1987)

The excitation-energy distribution of transition strength to 1^+ states excited via the $^{26}\text{Mg}(\text{p},\text{n})^{26}\text{Al}$ reaction at 134.4 MeV was measured for excitation energies up to 25 MeV. The structures observed in the neutron spectra with $\Delta L=0$ angular distributions were identified as 1^+ states, except for the isobaric analog transition. The total 1^+ strength in this reaction was extracted by normalizing the intensity of the four lowest 1^+ states to the strength measured for the analogous beta decays to these states. A detailed comparison of the experimental results with known analogous transitions and with a large-basis shell-model calculation leads to the conclusion that strengths to states of isospin $T=0, 1$, and 2 were observed in this reaction. The apportionment of the observed strength among the three isospin values is compared with the shell-model prediction. The total strength observed to all states below an excitation energy of 15 MeV is 57 percent of the total strength predicted by the shell-model calculation with the assumption of the "free-nucleon" normalization of the Gamow-Teller beta decay operator.

I. INTRODUCTION

Many studies of the (p,n) reaction at intermediate energies have been carried out to determine the strength function for Gamow-Teller (GT) transitions in the giant-resonance region. Generally, it is found that this (p,n) strength is quenched in the sense that about 60% of the expected sum-rule strength is found in discrete states in the region of excitation energy below about 15 MeV. Apparently, the missing strength is shifted to higher excitation energies, presumably through the influences of the tensor force, the delta resonance, and meson-exchange currents. The magnitude of each of these effects and the contribution of each to the missing strength is a problem of intense current interest; however, their quantitative determination from the experimental data can be made only if the standard nuclear physics of the problem is understood. Toward this end, it is necessary not only to know the effects of configuration mixing in the shell-model basis chosen for the problem, but also to ensure that the chosen basis is large enough to describe the mixing properly.

This problem can be approached by studying the effects of configuration mixing as a function of the isospin of the nuclear states involved. We compared large- and small-basis shell-model calculations for ^{26}Mg and found that the GT strength leading to $T=0$ states is relatively insensitive to configuration mixing, while that leading to $T=2$ states is relatively sensitive. This result indicates that studies of transitions to lower- T states should be particularly useful for the study of quenching phenomena and

that those to higher- T states should be particularly useful for the study of configuration mixing.

Since charge-exchange reactions on $N > Z$ nuclei with isospin T_0 can excite states with isospin T_0 and $T_0 \pm 1$, such reactions could be used for detailed studies of configuration mixing. Such studies are easier to carry out in nuclei with small neutron excesses because isospin geometry reduces the strengths of the higher isospin transitions¹ in nuclei with large neutron excess by factors of roughly $1/T_0$ and $(1/T_0)^2$. Also, since nuclear reactions do not provide a direct isospin meter, a combination of experimental results and theoretical analysis must be used to assign a given excitation to a given T . If this process is to succeed, a good theoretical model is required for the range of excitation involved. For these reasons, there are few, if any, cases where a convincing test of the distribution of GT strength with T was made. Even individual transitions that can be attributed convincingly to states of $T_0 + 1$ are rare.

We report here a study of the distribution of GT strength in the $^{26}\text{Mg}(\text{p},\text{n})^{26}\text{Al}$ reaction at 134.4 MeV; the good (~ 370 keV) resolution achieved permits the investigation of more structure at high excitation energies than was possible previously. The large-basis shell-model calculations available for ^{26}Al permit a detailed comparison with experimental results. Earlier work on this reaction at intermediate energies was performed by Goodman *et al.*² and at lower energies by Sterrenburg *et al.*³ and Berg *et al.*⁴ In another paper,⁵ a similar study is reported for the $^{58,60,62,64}\text{Ni}(\text{p},\text{n})$ reactions; in this case, isospin assignments were made based on the identification of T_0

and $T_0 + 1$ strength seen in (p,p') studies on the same isotopes.

A detailed comparison of the experimental results for ^{26}Mg with known analog transitions and with large-basis shell-model calculations leads to the conclusion that strengths to states of $T = 0, 1$, and 2 were observed in this reaction. The resulting experimental values are compared with shell-model predictions; we observe about 57% of the sum-rule strength, consistent with results on other nuclei.

II. EXPERIMENTAL PROCEDURE

The experiment was performed at the Indiana University Cyclotron Facility with the beam-slinger system.⁶ The beam slinger is capable of deflecting the incident proton beam through an angle of up to 26° . The neutrons were detected in mean-timed⁷ neutron detectors⁸ located 85.8 ± 0.2 m from the target and at 0° to the undeflected proton beam. The detector array consisted of three NE102 plastic scintillators, each 1.02 m long by 0.508 m high by 10.2 cm thick, with a total frontal area of 1.55 m^2 . Protons from the target were rejected by an anticoincidence detector in front of the array. Cosmic rays were vetoed by anticoincidence detectors on top and at the front of the array. The details of the electronics and data acquisition system are similar to those described previously.⁹

Neutron energies were measured by the time-of-flight (TOF) technique with an energy resolution [full width at half maximum (FWHM)] of 370 keV measured for 128.5 MeV neutrons at 0.3° . The magnesium metal target was $35.8 \pm 0.9 \text{ mg/cm}^2$ thick and was enriched to 99.45% ^{26}Mg . Time-of-flight spectra were measured at laboratory angles of 0.3° , 3.9° , 8.0° , and 11.6° . Spectra from each detector in the array were recorded at many pulse-height thresholds ranging from 25 to 90 MeV ee (MeV of equivalent electron energy). Calibrations of the pulse-height response of each of the detectors were performed with a ^{232}Th gamma source, which emits a 2.6 MeV gamma ray. During the experiment the calibration was checked periodically with this source and found to be stable to within 10%. The values of the cross sections extracted for several thresholds (from 40 to 70 MeV ee) were the same within statistics.

The energy resolution of 370 keV corresponds to a time dispersion of 730 ps. We estimate the contributions to the overall time dispersion to be (i) the intrinsic time dispersion of the neutron detectors (~ 300 ps), (ii) the beam-energy spread of about 0.1% (~ 270 ps), (iii) the finite target thickness (~ 450 ps), (iv) the finite thickness of the detector (~ 530 ps), and (v) the dispersion in the timing signal obtained from the cyclotron radio frequency (~ 350 ps). The overall time dispersion quoted is not the quadrature sum of these individual sources because the contributions from the thickness of the target and the detectors do not follow a Gaussian distribution; a proper folding of all five contributions predicts a resolution of 730 ps. Absolute cross sections were extracted with efficiencies calculated with the Monte Carlo code of Cecil *et al.*¹⁰ These efficiencies were checked¹¹ by comparing various (p,n) and (p,p') analog transitions. The overall neutron detection efficiencies determined in this way were tested previ-

ously to be accurate to better than $\pm 10\%$.^{11,12} Efficiencies obtained from the most recent measurement¹³ of the ^7Li (p,n) activation cross section are now consistent with these Monte Carlo efficiencies.

III. DATA REDUCTION

The neutron TOF spectra were converted to neutron-energy spectra with the large 1^+ state at an excitation energy in ^{26}Al of 1.06 MeV serving as the calibration point. Figure 1 shows the raw TOF spectrum measured at 0.3° ; Fig. 2 shows the corresponding excitation-energy spectrum without subtraction of any backgrounds. The inset in Figs. 1 and 2 is the portion of the excitation-energy spectrum above 12.5 MeV, rescaled to show the structure in this region better. Excitation energies in the final nucleus are determined to about 100 keV; the results are within 40 keV of published values for $E_x < 6$ MeV. Our measured spectrum is consistent with the spectrum of this reaction obtained previously² at 120 MeV bombarding energy with poorer energy resolution. The dominant features of the spectrum are the 0^+ isobaric analog state at 0.23 MeV and a pair of strong 1^+ peaks at 1.06 and 1.85 MeV excitation energy, a smaller cluster of strength centered about a moderately strong peak at 5 MeV, a complex structure of peaks in the region of 9–11.5 MeV excitation energy which embodies, in the aggregate, a significant fraction of the total observed intensity, and, finally, an isolated narrow peak at 13.6 MeV excitation energy.

The TOF spectra observed at the four angles were fitted to the sums of individual peak shapes in three separate regions of excitation energy (E_x): region I from 0 to 8 MeV region II from 8 to 13.3 MeV and region III from 13.3 to 25 MeV. We treated the continuum background in three different ways: (1) a calculated quasifree (p,pn) background, (2) a polynomial background for the entire spectrum, and (3) a separate polynomial background for each of the three regions. In the first method, the known

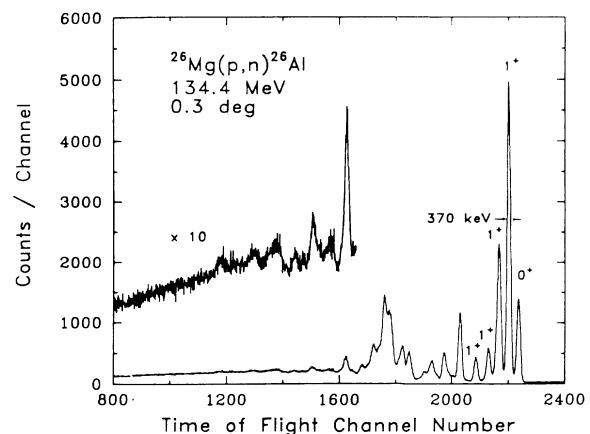


FIG. 1. Neutron time-of-flight spectrum at 0.3° from the $^{26}\text{Mg}(p,n)^{26}\text{Al}$ reaction at 134.4 MeV. This spectrum is for a software threshold of 50 MeV ee.

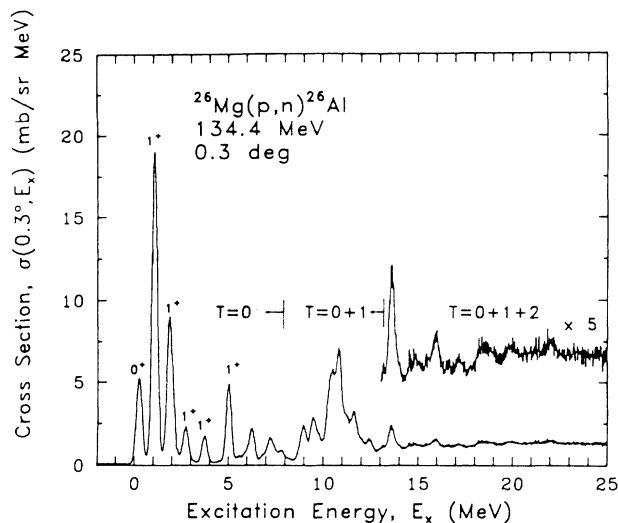


FIG. 2. Excitation-energy spectrum at 0.3° from the $^{26}\text{Mg}(p,n)^{26}\text{Al}$ reaction at 134.4 MeV. Regions where states of different isospins occur are noted. Inset is rescaled by a factor of 5.

cosmic-ray background and the overlap background from earlier beam bursts were removed before subtracting the quasifree spectrum. The quasifree background was calculated in a plane-wave impulse approximation with a modified version of a code written by Wu.¹⁴ These calculations were normalized (at each angle) to account completely for the continuum at a neutron energy of 90 MeV ($E_x = 39.3$ MeV). This procedure is similar to that used for the ^{40,48}Ca(p,n) reactions by Anderson *et al.*¹⁵ In the second method, a different line shape was used for the peaks in each region and the entire spectrum was fitted simultaneously with the background. The line shapes for each region are discussed below. In the third method, the peaks in each region were fitted simultaneously with the background in that region. The spectrum from Fig. 1 is replotted in Fig. 3 to show the three methods of background subtraction. The third technique, which does not provide a continuous background from one region to the next, yielded cross sections which were consistently smaller than those obtained with either of the other two methods; for example, cross sections extracted with the third method were as much as 50% smaller for states in region III. Although the third method has discontinuities which are unphysical, it represents an upper limit which overestimates the background in a region (such as region III) with broad and overlapping peaks. The difference in cross sections obtained with methods (1) and (2) was always less than 8% in region I, 13% in region II, and 20% in region III. Because methods (1) and (2) yield similar results, and because method (1) is based on a model for the observed background, we adopt the results from method (1) as our best determination.

Since the states in the first region of the ^{26}Al spectrum are bound (for $E_x < 6.3$ MeV), the widths of the peaks in this region should be due primarily to instrumental factors; accordingly, this region was fitted with Gaussian line

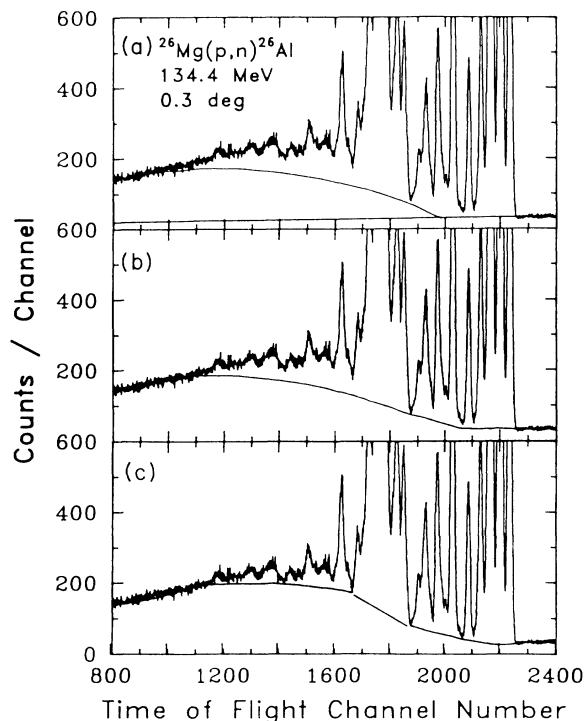


FIG. 3. Neutron time-of-flight spectrum at 0.3° showing (a) the quasifree background and the overlap plus cosmic-ray backgrounds, (b) the polynomial background for the entire spectrum, and (c) the polynomial backgrounds for three individual regions.

shapes of equal (time) widths as shown in Fig. 4 (with the first method of background subtraction). In this region, 12 peaks at excitation energies listed in Table I, were observed with angular distributions peaked at 0° and thereby identified as $\Delta L=0$ transitions; in addition, five peaks (at $E_x=3.10, 4.55, 5.55, 7.51$, and 8.28 MeV) were found to have angular distributions that are not peaked at 0° . Six of the twelve $\Delta L=0$ transitions correspond to known 1^+ states in ^{26}Al ; that at $E_x=228$ corresponds to the analog of the 0^+ ground state of ^{26}Mg .

Since all of the states in both the second and third regions of the ^{26}Al spectrum are unbound, they were fitted with Breit-Wigner line shapes except for the narrow isolated peak at 13.6 MeV, which was fitted with a Gaussian line shape with a width that is essentially the same as the instrumental resolution. Constant (time) widths were used for the second region. The peaks in the third region were fitted best with two sets of widths, one width of about 30 channels for six peaks at excitation energies from 14.6 to 17.2 MeV and a larger width of about 50 channels for eight peaks at higher excitation energies from 18.3 to 23 MeV. The time calibration was 45.68 ps/channel. Shown in Figs. 5 and 6 are the fitted time-of-flight spectra for these two regions after subtraction of the cosmic-ray, overlap, and quasifree backgrounds. Eight peaks in the second region, with excitation energies listed in Table I,

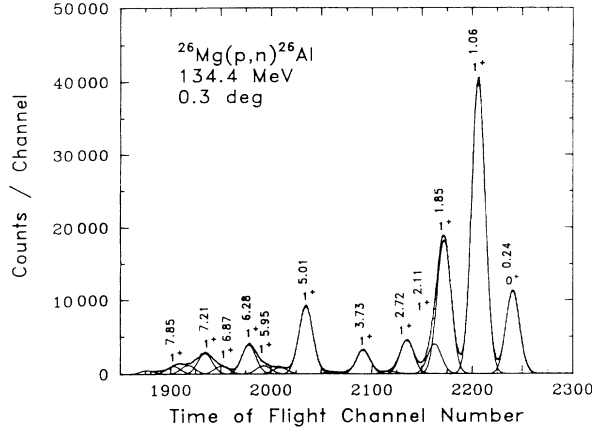


FIG. 4. The $T=0$ region of the neutron time-of-flight spectrum at 0.3° from the $^{26}\text{Mg}(p,n)^{26}\text{Al}$ reaction at 134.4 MeV after subtraction of quasifree, overlap, and cosmic-ray backgrounds. The solid lines were generated with a peak-fit code. Excitation energies shown result from the fit. This spectrum is for a software threshold of 25 MeV ee.

were observed with $\Delta L=0$ angular distributions; four peaks (at $E_x=9.45$, 12.01, 12.42, and 12.80 MeV) were found to have angular distributions that are not $\Delta L=0$. Region III is dominated by the $\Delta L=1$ giant resonances. Much of the strength observed at 0° in this region has a $\Delta L=1$ angular distribution. The background in this region consists of strong contributions from both the $\Delta L=1$ giant resonance and quasifree (p,pn) scattering. Although this fitted background is probably not a good representation of these strengths, it allows one to extract the strength of the small peaks in this region correspond-

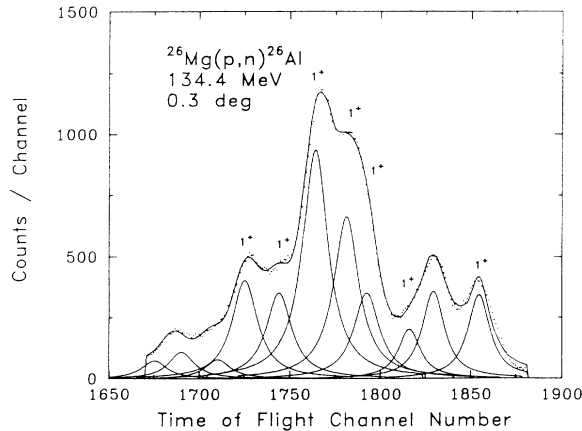


FIG. 5. The predominantly $T=1$ region of the neutron time-of-flight spectrum at 0.3° from the $^{26}\text{Mg}(p,n)^{26}\text{Al}$ reaction at 134.4 MeV after subtraction of quasifree, cosmic-ray, and overlap backgrounds. The solid lines were generated with a peak-fit code. This spectrum is for a software threshold of 25 MeV ee.

TABLE I. Excitation-energy distribution of the $\Delta L=0$ cross sections in the $^{26}\text{Mg}(p,n)^{26}\text{Al}$ reaction at 134.4 MeV and 0.3° . An asterisk indicates unresolved peaks. Statistical uncertainties are greater than those for other individual peaks which have statistical uncertainties that are typically less than 3%.

Excitation energy E_x (MeV)	Momentum transfer q (fm $^{-1}$)	Cross section (mb/sr) $\sigma(q)$
Compilation ^a	Peak fitting ^b	
Region I [$0 \leq E_x$ (MeV) ≤ 8]		
0.228	0.24	2.02
1.058	1.06	7.43
1.850	1.85	3.36
2.072	2.11	0.70*
2.739	2.72	0.87
3.723	3.73	0.63
5.006	5.01	1.80
(5.91)	(5.95)	0.25*
	(6.28)	0.78
	(6.87)	0.19*
	(7.21)	0.54
	(7.85)	0.26*
Region II [$8 \leq E_x$ (MeV) ≤ 13.3]		
	(8.94)	0.94
	(9.77)	0.56*
	(10.2)	0.96*
	(10.5)	1.81
	(10.8)	2.61
	(11.2)	1.00
	(11.6)	1.13
	(13.1)	0.26*
Region III [$13.3 \leq E_x$ (MeV) ≤ 25]		
	(13.6)	0.69
	(14.6)	0.59*
	(14.9)	0.36*

^aReference 31.

^bParentheses indicate that the excitation energies extracted from the peaks may represent an average over more than one state.

ing to $\Delta L=0$ transitions. In Region III we observe three peaks at excitation energies listed in Table I with $\Delta L=0$ distributions, seven peaks (at $E_x=15.55$, 15.93, 16.63, 18.32, 20.07, 21.03, and 22.12 MeV) that appear to have some $\Delta L=0$ strength, and six peaks (at $E_x=13.80$, 17.17, 18.73, 19.76, 21.57, and 23.00 MeV) that appear to have no $\Delta L=0$ strength appear to be unresolved complexes of states with $\Delta L=0$ and 1 transitions.

IV. RESULTS

We extracted the angular distributions for each peak observed in the 0° spectrum, identified $\Delta L=0$ transitions to levels in ^{26}Al with excitation energies up through 25 MeV, extracted the intensity, and estimated the Gamow-Teller strength for each $\Delta L=0$ transition. Independent spectroscopic evidence (see below) permits assigning isospin $T=0$ to the lowest few states in ^{26}Al ; however, the remainder of the observed strength in ^{26}Al cannot be as-

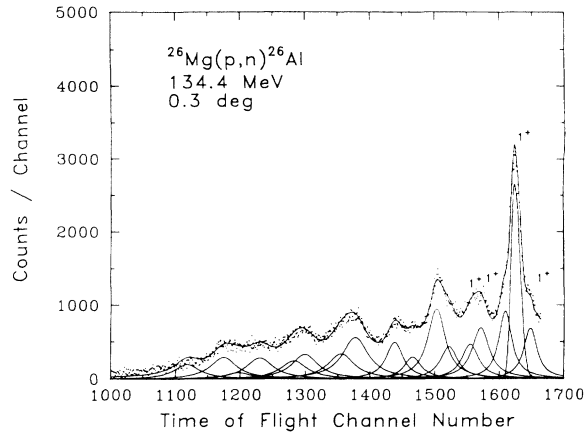


FIG. 6. The high-excitation region of a neutron time-of-flight spectrum at 0.3° from the $^{26}\text{Mg}(p,n)^{26}\text{Al}$ reaction at 134.4 MeV after subtraction of quasifree, cosmic-ray, and overlap backgrounds. The solid lines were generated with a peak-fit code. The narrow isolated peak at 13.6 MeV was fitted with a Gaussian line shape with a width essentially equal to the instrumental resolution; the other peaks were fitted with Breit-Wigner line shapes. This spectrum is for a software threshold of 25 MeV ee.

signed rigorously to a specific isospin.

The extracted angular distributions for the strongest 1^+ transition (viz., to the state at $E_x = 1.06$ MeV) and for the 0^+ (isobaric-analog-state) (IAS) transition are presented in Fig. 7. The excitation energies and cross sections of the $\Delta L = 0$ transitions observed in the 0° spectrum are listed in Table I. At 0° , the contribution from transitions with $\Delta L = 1$ is generally small in regions I and II and does not affect appreciably the extraction of $\Delta L = 0$ strength in these two regions. The angular distributions for the two largest $\Delta L = 0$ transitions in the second region are presented in Fig. 8. The strongest $\Delta L = 0$ transition in the excitation energy region above 13 MeV is to a state at $E_x = 13.6$ MeV (see Figs. 1, 2, and 6). The angular distribution extracted for this transition is presented also in Fig. 8. The solid lines in Figs. 7 and 8 are the results of distorted-wave impulse-approximation (DWIA) calculations performed with the code DW81.¹⁶ These calculations use the effective interaction of Franey and Love at 140 MeV,¹⁷ the optical-model potentials of Olmer *et al.*,⁸ and harmonic-oscillator wave functions from Brown.¹⁹

The absolute cross sections for these transitions were extracted from the known target thickness, beam-charge integration, calculated neutron-detection efficiencies, and measured solid angle. The beam charge was measured with a well-shielded split Faraday cup located approximately 10 m downstream from the target. The uncertainty in the target thickness is given above. The beam integration is estimated to be accurate to $\pm 5\%$. The uncertainty in the calculated detection efficiencies is estimated to be about 11%, which is a quadrature sum of about 5% from the Monte Carlo code and about 9% from threshold uncertainties. The uncertainty in the solid angle is due

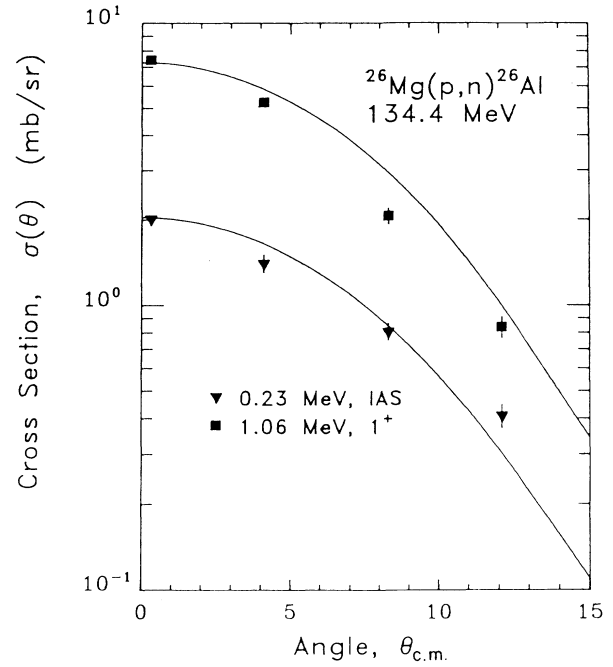


FIG. 7. The differential cross section vs the center-of-mass angle for the transitions to the IAS state at 0.23 MeV and to the largest 1^+ state at 1.06 MeV in ^{26}Al from the $^{26}\text{Mg}(p,n)^{26}\text{Al}$ reaction at 135 MeV. The solid lines are DWIA calculations (see text for details).

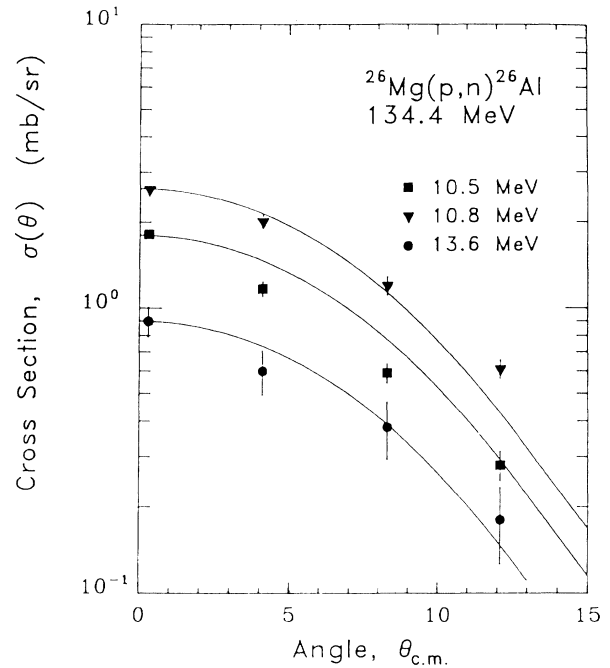


FIG. 8. The differential cross section vs the center-of-mass angle for the transitions to the two largest $T=1$ states in ^{26}Al (at 10.4 and 10.8 MeV) and for the transition to the largest $T=2$ state in ^{26}Al (at 13.6 MeV) from the $^{26}\text{Mg}(p,n)^{26}\text{Al}$ reaction at 135 MeV. The solid lines are DWIA calculations (see text for details).

largely to the ± 0.2 m uncertainty in the measured flight path, which corresponds to an uncertainty in the solid angle of less than 0.5%. The differential cross sections were corrected for the attenuation of the neutron flux in transit from the target to the detectors and for the computer lifetime; the calculation of the attenuation is estimated to be accurate to better than $\pm 5\%$, and the livetime is estimated to be known to better than $\pm 1\%$. The systematic uncertainty in the cross sections estimated from all of these sources is $\pm 13\%$. Statistical uncertainties of the individual peaks listed in Table I are typically less than 3%; however the cross sections with an asterisk have significantly higher uncertainties because those peaks are not resolved from other peaks.

V. GAMOW-TELLER STRENGTH

The total GT strength observed in this reaction can be extracted by normalization of the intensity of the four lowest 1^+ transitions to the intensity measured for the analog beta decays. The $^{26}\text{Mg}(p,n)^{26}\text{Al}$ reaction is the analog of the β^+ decay of ^{26}Si to ^{26}Al . The $\log ft$ values for the beta decays to the states at excitation energies of 1.058, 1.850, 2.0972, and 2.739 MeV in ^{26}Al are 3.550, 3.855, 4.629, and 4.539, respectively.²⁰ It is possible to extract the GT matrix element for these decays from the relationship between Fermi (F) and GT matrix elements and observed ft values,²¹

$$B(F) + \left[\frac{g_A}{g_V} \right]^2 B(\text{GT}) = \frac{6170 \pm 4}{ft}. \quad (1)$$

Values of g_A/g_V obtained by Wilkinson,²² Freedman,²³ and Kajino *et al.*²⁴ are 1.2605 ± 0.0075 , 1.262 ± 0.0055 , and 1.2642 ± 0.0062 , respectively. For $g_A/g_V = 1.262$ and for a pure GT transition, Eq. (1) becomes

$$B(\text{GT}) = 3874/ft. \quad (2)$$

Equations (1) and (2) are expressed in units such that the beta decay of the free neutron has a value $B(\text{GT}) = 3$. The $B(\text{GT})$ values obtained from Eq. (2) are 1.092, 0.541, 0.091, and 0.112, respectively, for the beta decays to the four lowest-lying GT states. These values are listed in Table II in the right-hand column headed $B_\beta(\text{GT}, q=0)$. The notation $q=0$ is used because the beta-decay $B(\text{GT})$ values are measured at a momentum transfer of nearly zero; accordingly, the 0.3° cross sections from the (p,n) reaction must be extrapolated to $q=0$ (or to the smallest kinematically allowed q) before converting the cross sections to $B_{\text{pn}}(\text{GT})$ values. This extrapolation is performed with a shape calculated by the DWIA for a $\Delta L=0$ transition. The values of the cross section extrapolated to the kinematic-minimum momentum transfer $q=0.05 \text{ fm}^{-1}$ ($\sim 10 \text{ MeV}/c$) are listed in Table II in the third column. The ratio of the sum of the $B_\beta(\text{GT}, q=0)$ values for the first four GT states to the sum of the (p,n) cross sections at 0° for these states is used to extract the matrix elements $B_{\text{pn}}(\text{GT}, q=0.05 \text{ fm}^{-1})$ associated with all of the measured 0° (p,n) cross sections for GT transitions. The individual values are listed in Table II in the fourth column. The sum of the matrix elements for GT states with excita-

tion energies from 1 to 15 MeV is 4.41.

Based on the assumption that only nucleon degrees of freedom are important in the nucleus, the sum rule for Gamow-Teller beta decay is²⁵

$$S(\beta^-) - S(\beta^+) = 3(N - Z), \quad (3)$$

where

$$S(\beta^\pm) = \sum B(\text{GT}^\pm). \quad (4)$$

Here the sum is on all β^- or β^+ transitions from the ground state. Then we have $S(\beta^-) \geq 3(N - Z)$, where the equality holds when $S(\beta^+) = 0$ (i.e., when β^+ decays are blocked). For ^{26}Mg , these decays will not be negligible. With the above units for $B(\text{GT})$, we have the model-independent result that

$$S(\beta^-) \geq 6. \quad (5)$$

From our results (summarized in Table II) that $\sum B_{\text{pn}}(\text{GT}) = 4.41$, the GT strength $S(\beta^-)$ observed in discrete states amounts to 73% of the $3(N - Z)$ sum rule limit for ^{26}Mg . This fraction must be reduced further by the still undetermined strength $S(\beta^+)$ in the β^+ decay channel. In order to use Eq. (3), it is necessary to invoke a model to estimate $S(\beta^+)$; for example, the shell-model calculation discussed in the next section yields the result that $S(\beta^+) = 1.78$; hence, the $\sum B_{\text{pn}}(\text{GT})$ value of 4.41 represents 57% of the sum rule equation (3).

It is interesting to note here that a lower limit for $S(\beta^+)$ may be deduced from the measured (p,n) cross section for the state at $E_x = 13.6 \text{ MeV}$, which is the lowest $T=2, 1^+$ state in the spectrum of ^{26}Al , as discussed in Sec. VIC. This $T=2$ state in ^{26}Al is the analog of the first 1^+ state of ^{26}Na , presumed to occur at an excitation energy of 0.088 MeV, as discussed in Sec. VIC. Since the ratio of the (n,p) cross section to the (p,n) cross section is given by the square of the ratio of the isospin Clebsch-Gordan coefficient for the (n,p) reaction to that for the (p,n) reaction, the reduced transition probability for the β^+ transition to the $T=2$ state in ^{26}Na is given by

$$B(\text{GT}^+) = 6B(\text{GT}^-).$$

Here the factor 6 is the square of the ratio of the Clebsch-Gordan coefficients. The Clebsch-Gordan coefficient for the $^{26}\text{Mg}(n,p)^{26}\text{Na}$ reaction is unity; that for the $^{26}\text{Mg}(p,n)^{26}\text{Al}$ reaction is $(\frac{1}{6})^{1/2}$. Since $B(\text{GT}^-) = 0.12$ for the $T=2$ state in ^{26}Al , $B(\text{GT}^+) = 0.72$. Hence, the observed $\sum B_{\text{pn}}(\text{GT}^-) = 4.41$ represents less than $4.41/6.72 = 66\%$ of the sum rule strength. Additional (n,p) transitions from the ^{26}Mg ground state to states in ^{26}Na at higher excitation energies will increase $S(\beta^+)$ and reduce further the percentage of the sum-rule strength observed.

We examined the possibility that part of the strength seen in the 13.6 MeV peak might come from carbon contamination of the target. Since Q values are -18.13 and -4.786 MeV , respectively, for the $^{12}\text{C}(p,n)^{12}\text{N}$ and $^{26}\text{Mg}(p,n)^{26}\text{Al}$ ground-state reactions, the $^{12}\text{N}(\text{g.s.})$ peak would appear in the ^{26}Al spectrum at an excitation energy of 13.34 MeV, which is between the 13.6 and 13.1 MeV peaks and within our ability to determine excitation ener-

TABLE II. Excitation-energy distribution of the Gamow-Teller (GT) strength from the $^{26}\text{Mg}(\text{p},\text{n})^{26}\text{Al}$ reaction at 134.4 MeV.

Excitation energy E_x (MeV)		Extrapolated ^a cross section $\sigma(q=0.05 \text{ fm}^{-1})$ (mb/sr)	GT strength		
Expt. ^b	Theor.		$B_{\text{pn}}(\text{GT})$ $q=0.05 \text{ fm}^{-1}$	$B_{\text{theor},0.57(\text{GT})}$	$B_{\beta}(\text{GT})$ $q=0$
0.24		2.10	0^+ IAS		
1.06	0.965	7.73	1.10	1.08	1.092
1.85	1.884	3.52	0.50	0.49	0.541
2.11	2.150	0.74	0.11	0.10	0.091
2.72	3.046	0.93	0.13	0.07	0.112
Sum		12.92	1.84	1.74	1.836
(first four GT states)					
3.73	0.68	0.10			
5.01	1.95	0.28			
(5.95)	0.28	0.04			
(6.28)	0.86	0.12			
(6.87)	0.21	0.03			
(7.21)	0.61	0.09			
(7.85)	0.29	0.04			
$[0 \leq E_x(\text{MeV}) \leq 8]$	(17.80)	(2.54)	(2.30) ^d		
(8.94)	1.08	0.15			
(9.77)	0.65	0.09			
(10.2)	1.14	0.16			
(10.5)	2.15	0.31			
(10.8)	3.12	0.44			
(11.2)	1.20	0.17			
(11.6)	1.37	0.20			
(13.1)	0.33	0.05			
$[8 \leq E_x(\text{MeV}) \leq 13.3]$	(11.04)	(1.57)	(1.58) ^e		
13.6	0.87	0.12	0.08		
(14.6)	0.76	0.11			
(14.9)	0.47	0.07			
$[13.3 \leq E_x(\text{MeV}) \leq 15]$	(2.10)	(0.30)	(0.23) ^f		
$[0 \leq E_x(\text{MeV}) \leq 15]$	30.94	4.41 ^d	4.12		

^aExtrapolated with the DWIA to the kinematic-minimum momentum transfer.^bParentheses indicate that the excitation energies extracted from the peaks may represent an average over more than one state.^cThis value is 73% of $3(N-Z)$ and 57% of the sum rule given in Eq. (3) when $S(\beta^+)$ is taken from the shell model. The present shell-model prediction for the β^+ strength is given by the product of the value of 0.297 predicted in column 3 of Table III for the β^- strength to the isobaric analog ($T=2$) state and an isospin Clebsch-Gordan factor of 6; that is $6 \times 0.297 = 1.78$. The value of 57% obtained here from the (p,n) measurement is coincidentally the same as that obtained from the survey of beta decay.^dConsists of 2.29 ($T=0$) and 0.01 ($T=1$).^eConsists of 0.35 ($T=0$) and 1.23 ($T=1$).^fConsists of 0.06 ($T=0$), 0.08 ($T=1$), and 0.09 ($T=2$).

gies to about 100 keV. Even if the target were contaminated with carbon, we estimate that such contamination cannot contribute significantly to the strength of the 13.6 MeV state; more specifically, based on our estimate that the contribution from carbon contamination, if any, to strength at 13.3 MeV is less than half of that for the peak at 13.1 MeV, potential carbon contamination would contribute less than 10% to the strength of the 13.6 MeV states. It should be noted that an unrealistically large carbon contamination of about $70 \mu\text{g}/\text{cm}^2$ is required to pro-

duce a peak at 13.3 MeV with a strength equal to half of that at 13.1 MeV, which we could see. Also, a search at angles away from 0° for the 4^- state at $E_x = 4.4$ MeV in ^{12}N was unable to reveal a presence of carbon contamination of the target because of interference with a high-spin (6^- and 4^-) complex in ^{26}Al .

Also, we note that extraction of GT strength in the $T=2$ region is not affected by a possible contamination of the target with oxygen. In the $^{16}\text{O}(\text{p},\text{n})^{16}\text{F}$ reaction at 135 MeV, strongly excited peaks with $J^\pi = 2^-$ were ob-

served²⁶ at excitation energies of 0.4 and 7.6 MeV in ¹⁶F. Since the Q value for the ¹⁶O(p,n)¹⁶F reaction is -16.2 MeV, the apparent excitation energies would correspond to 11.8 and 19.0 MeV in ²⁶Al; however, 1^+ peaks were not observed at either of these two excitation energies.²⁶ Also, as noted earlier, the peaks observed in ²⁶Al at 18.7 and 19.8 MeV both appear to have no $\Delta L = 0$ strength.

VI. COMPARISON WITH SHELL-MODEL CALCULATIONS

A. Comments on the model

We compared these experimentally determined strengths and excitation energies for the Gamow-Teller transitions from ²⁶Mg to ²⁶Al with predictions obtained from the relevant $A=26$ members of a family of shell-model wave functions for the complete $A=17-39$ region.²⁷ These wave functions yield predictions of many of the observed spectroscopic features of nuclei in this mass region. The calculations that produced these wave functions incorporate the complete set of $0d_{5/2}$, $1s_{1/2}$, and $0d_{3/2}$ basis vectors for each A value and a single, shell-wide formulation of the model Hamiltonian. Thus, the predictions for $A=26$ are tied firmly to the overall spectroscopic properties of the entire surrounding region of nuclei. Alternate versions of shell-model predictions for Gamow-Teller strength to the levels of ²⁶Al were reported previously.^{28,29} The model Hamiltonian used to obtain the present results yields a better description for the energies and strengths of states in $A=26$ and neighboring nuclei than do previously available models; moreover, in contrast to the results of Ref. 29, the present predictions are obtained in all instances from fully converged eigenfunctions which have good J and T and which span the complete, untruncated, sd -shell model space. Some of the numerical values of predicted energies and strengths are presented in Tables II and III and will be discussed further below.

B. General and specific properties of the theoretical GT spectrum

Comparisons of the observed distribution of “giant resonance” strength with theoretical predictions can be made at different levels of detail. The state-by-state comparison which is conventional for the spectroscopy of low-lying states cannot be pursued much beyond 6 MeV of excitation energy. From 0 to 6 MeV the individual observed

strengths and their summed strengths are, as noted in Table II, in good agreement with the shell-model predictions scaled down by the factor of 0.57. Above 6 MeV excitation in this system, state-by-state correspondence and comparisons cannot be established. Experimental resolution is inadequate to identify every 1^+ state at higher energies. The number of experimental 1^+ states must inevitably rise above the number predicted in the one-major-shell model space because of the intrusion of non- sd -shell excitations. Also, as the level densities increase, the detailed ordering of states will be beyond the predictive capabilities of the model Hamiltonian, with its inherent accuracy of ± 150 keV.

Meaningful comparisons can still be made in this “statistical” region above 6 MeV by focusing on the total amount of strength and its distribution with excitation energy on scales of from 0.3 to 1.5 MeV. The experimental resolution of 370 keV provides a reasonable scale for the “fine structure” of the distribution. In Fig. 9 we compare the experimental strength replotted in 350 keV bins with the theoretical spectrum similarly binned and scaled by 0.57. The gross (1.5 MeV wide) structure of the distributions, with strength clustered at 1–2, 5–6, and 9–12 MeV, can be seen in both plots. At the 350 keV level of detail some differences between theory and experiment can be discerned, particularly in the 9–12 MeV region, where the model strength has a double-peaked distribution and experiment a single central peak.

The gross distributions in energy and the total amounts of observed and predicted strength are best seen in the integral representations of Fig. 10. Here the total amount of strength predicted (solid line) and observed (dashed line) below a given excitation energy is plotted as a function of this energy. Again, the predictions have been scaled by a factor of 0.57. From Fig. 10 we see that the total strength observed up to 15 MeV is close to the 0.57 scaling of the theory.

The choice of the reduction factor of 0.57 [which, coincidentally, is the same as that obtained here from the (p,n) studies] followed the results of a survey of Gamow-Teller beta decay. The family of $0d_{5/2}$, $1s_{1/2}$, $0d_{3/2}$ shell-model wave functions which yielded the present $A=26$ predictions was used to calculate the Gamow-Teller strengths for all observed beta decays in the $A=17-39$ region.³⁰ It was found that the assumption of the free-nucleon (FN) normalization of the GT operator yields theoretical strengths which, averaged over more than 200 pieces of data, are larger than experiment by a factor

TABLE III. Apportionment of Gamow-Teller strength from the ²⁶Mg 0^+ , $T=1$ ground state between the $T=0, 1$, and 2 isospin channels in ²⁶Al.

T	$B_{jj, \text{FN}}(\text{GT})$ (total)	$B_{\text{theor, FN}}(\text{GT})$ (total)	$B_{\text{theor, FN}}(\text{GT})$ ($E_x < 15$ MeV)	$B_{\text{theor, 0.57}}(\text{GT})$ ($E_x < 15$ MeV)	$B_{\text{pn}}(\text{GT})$
0	6.533	4.887	4.765	2.70	2.95
1	4.800	2.598	2.331	1.32	1.33
2	1.067	0.297	0.165	0.09	(≥ 0.12) (≤ 0.30)
Sum	12.400	7.782	7.261	4.12	

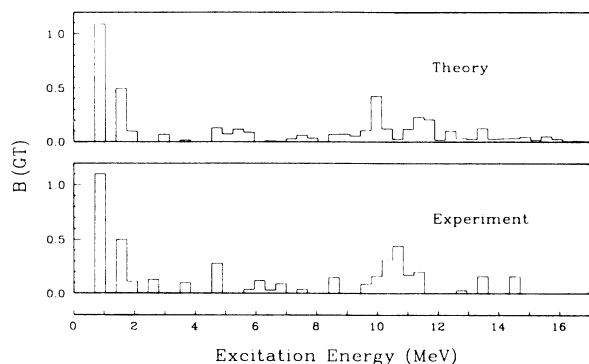


FIG. 9. Predicted and observed GT strength for the $^{26}\text{Mg}(p,n)^{26}\text{Al}$ reaction plotted in 0.35 MeV bins. The theoretical strength is scaled by a factor of 0.57. Energies are plotted relative to the 0^+ $T=1$ state.

$$B(\text{GT})_{\text{theor, FN}}/B(\text{GT})_{\text{expt}} = 1.76 \pm 0.14.$$

This factor differs slightly from the value of Ref. 30 because of the difference in the value of g_A/g_V used there (1.251) and here (1.262). This result motivates the scale factor of 0.57 ($=1/1.76$), which yields the lower (solid) curve in Fig. 10. The calculated GT spectrum for ^{26}Al obtained with this empirical normalization agrees qualitatively with the experimental spectrum from the $^{26}\text{Mg}(p,n)^{26}\text{Al}$ reaction at the level of detail specified by the 350-keV energy averaging.

Two essential features emerge from the comparison of experiment and theory shown in Fig. 9: (1) the total experimental GT strength obtained from the $^{26}\text{Mg}(p,n)^{26}\text{Al}$ reaction is close to 0.57 of the strength predicted by the present shell-model calculations for the region of observation under the assumption of the free-nucleon normalization of the GT operator, and (2) the calculated apportionment of this strength into three distinct regions of excita-

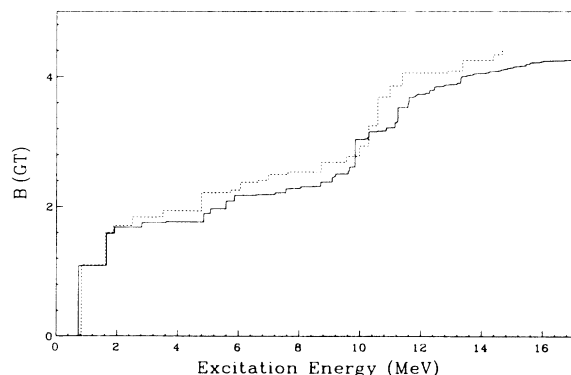


FIG. 10. The accumulating sum of the GT strength below a given excitation energy in ^{26}Al for the $^{26}\text{Mg}(p,n)$ reaction. The dashed line represents the (p,n) experimental results of Table II. The solid line is the theoretical prediction scaled by a factor of 0.57. Energies are plotted relative to the 0^+ , $T=1$ state.

tion energy, and the relative strengths of the regions, agree closely with the experimental results.

The isospin of the model state associated with each individual component of theoretical GT strength is, of course, known. Inspection of the details of the theoretical spectrum reveals that (1) the concentrations of strength predicted at 1 and 5 MeV excitation energy correspond to population of $T=0$ levels, (2) the dominant contributions to the broad structure at 9–11 MeV excitation energy are from population of $T=1$ levels, and (3) the strength at 13.6 MeV excitation corresponds to the population of the first 1^+ level with $T=2$. Specifically, as shown in Table II, the total strength of 2.30 predicted below 8 MeV excitation energy is more than 99% $T=0$, the total strength of 1.58 predicted between 8 and 13.3 MeV excitation energy is 78% $T=1$, and the dominant peak in the 13.3–15 MeV region, which is associated with the lowest $T=2$ state, is predicted to contain 0.08 out of a total of 0.23 units of strength in this region. This predicted structure of the theoretical curve is consistent with much of what is known or can be inferred on empirical grounds about the structure of the experimental strength distribution, as we discuss next.

C. Experimental information on isospin assignments in ^{26}Al

The low-lying energy-level³¹ spectrum of ^{26}Al is a combination of $T=0$ and 1 states, the $T=1$ states being isobaric analogs of states in the spectrum of ^{26}Mg . The excitation energy in ^{26}Al of the analog of the ^{26}Mg ground state is 0.228 MeV. Analogs of the excited states of ^{26}Mg , which can be identified in ^{26}Al , occur also in ^{26}Al at excitations roughly 0.23 MeV higher than their ^{26}Mg values. The first possible $T=1$, 1^+ state in the ^{26}Mg spectrum occurs at an excitation energy of 5.69 MeV; therefore, its analog should occur in ^{26}Al at an excitation energy of about 5.92 MeV. All of the strength below this excitation energy must thus correspond to excitation of $T=0$ levels.

An estimate of the excitation energy of the lowest $T=2$ state in ^{26}Al can be derived from the known masses³² of ^{26}Na (binding energy of $208\,156 \pm 16$ keV) and ^{26}Mg (binding energy of $216\,682 \pm 1$ keV) and the systematics of Coulomb displacement energies obtained from the lighter isotopes of Mg and Na, which have known analog-state correspondence. From these systematics, we estimate a Coulomb shift of 4700 ± 50 keV between ^{26}Mg and ^{26}Na and hence an excitation energy in ^{26}Mg of 13.23 ± 0.06 MeV for the analog of the ^{26}Na ground state. This state in ^{26}Al should occur, then, at an excitation energy of 13.46 ± 0.06 MeV. The spin parity of the ^{26}Na ground state is known to be 3^+ . A spectrum of ^{26}Na is available from the $^{26}\text{Mg}(t, {}^3\text{He})^{26}\text{Na}$ reaction.³³ These data require energy levels at excitation energies of 0.088, 0.241, 0.420, (1.996), 2.048, 2.186, . . . MeV; the parentheses indicate that this excitation energy probably corresponds to the centroid of a doublet. The analogs of these states should appear in ^{26}Al at excitation energies appropriately shifted up from the ^{26}Na ground-state analog energy. On this basis, the lowest possible 1^+ state with $T=2$ could appear in the spectrum of ^{26}Al at an ex-

citation energy of 13.55 ± 0.06 MeV.

We noted above that a significant feature of the experimental $^{26}\text{Mg}(p,n)^{26}\text{Al}$ spectrum was an isolated peak at an excitation energy of 13.6 MeV with a width essentially equal to our instrumental resolution. This peak corresponds to a strong $M1$ state observed by Bendel *et al.*³⁴ from backward-angle electron scattering by ^{26}Mg . The strength and narrow width of this peak, and its separation from the lower-lying strength, combine with its measured excitation energy to suggest strongly that this peak corresponds to the population of the lowest 1^+ , $T=2$ state in ^{26}Al . Since this state is above the threshold for neutron emission, its narrow width suggests that neutron decay is forbidden by isospin, as would be expected for a $T=2$ state. The present shell-model calculation predicts an excitation energy in ^{26}Al for this lowest 1^+ , $T=2$ state of 13.309 MeV and a relatively large GT strength; however, with the 0.57 quenching factor applied, the predicted strength is slightly smaller than that measured for the 13.6 MeV peak. Thus, our assumption of $T=2$ for the 13.6 MeV peak is consistent, given some uncertainty about its strength, with both known analog $T=2$ states and the theoretical expectations.

D. Relative distribution of GT strength over different isospins

The apportionment of the GT strength from the $T=1$ ground state of ^{26}Mg between the three possible isospin channels in ^{26}Al depends sensitively upon the mixing in the target wave function of the three sd -shell orbitals. The predicted apportionment can be quoted either in terms of the strengths to states falling within the region of measured excitation energies or in terms of the strengths to all states in the model space. In fact, the choice between these alternatives is not crucial, since more than 90% of the predicted strength occurs within the region of observation.

We present in Table III predictions and observations on the apportionment of GT strength between the $T=0$, 1, and 2 channels. The second column of Table III lists the strengths which would be obtained if the wave function of ^{26}Mg was assumed to correspond to the j - j coupling limit of ten $0d_{5/2}$ nucleons coupled to $J=0$, $T=1$. The third column lists the sums of GT strength from the correlated ground-state wave function obtained for ^{26}Mg (0^+) in Ref. 26 to all model states of $T=0$, 1, and 2. The fourth column lists the sums of these strengths for all the states which fall within the first 15 MeV of excitation energy. These strengths correspond to the use of the free-nucleon normalization of the GT operator. Comparison of the entries in the third and fourth columns illustrates the concentration of strength into the low-excitation-energy portion of the ^{26}Al spectrum.

With reference to the second column, we see that the effects of the configuration mixing induced by the Hamiltonian upon the total strengths vary markedly with T . The $T=0$ strength is reduced from the j - j coupling limit by a factor of 0.75, the $T=1$ strength by a factor of 0.54, and the $T=2$ strength by a factor of 0.28. (The sum of the strengths in the three isospin channels is reduced by a

factor of 0.63). This comparison shows that the $T_f=T_i-1$ strengths are least sensitive to the details of the model Hamiltonian and hence provide the best ground for investigations of issues such as the systematic quenching of GT strength by effects not included in the theoretical calculation. Likewise, the $T_f=T_i+1$ strengths are most sensitive to Hamiltonian-induced effects and hence are best suited as a probe of the correct shell-model structures of these systems.

In the fifth column of Table III, we list the values of the fourth column multiplied by 0.57, and, in the sixth column, the estimates for the corresponding measured strengths. The agreement between the entries of these last two columns is seen to be good overall. Estimates for both $T=0$ and 1 strength are obtained by weighting the experimental values for the appropriate excitation energy regions demarked in Table II by the predicted ratios of strength for the various isospins in these regions. In the lowest excitation energy region [$0 \leq E_x(\text{MeV}) \leq 8$], the contribution from $T=1$ states is only 0.01 compared to the total $B_{\text{theor},0.57}(\text{GT})=2.30$; in the middle excitation energy region [$8 \leq E_x(\text{MeV}) \leq 13.3$], the value of 1.58 for the total $B_{\text{theor},0.57}(\text{GT})$ comprises 0.35 from $T=0$ states and 1.23 from $T=1$ states; and in the highest excitation energy region [$13.3 \leq E_x(\text{MeV}) \leq 15$], the value of 0.23 for the total $B_{\text{theor},0.57}(\text{GT})$ consists of 0.06 from $T=0$ states, 0.08 from $T=1$ states, and 0.09 from $T=2$ states. To estimate the $T=2$ strength, we simply give the range of values consistent with the data: the lower bound follows from assuming only the 13.6 MeV state has $T=2$, and the upper bound from assuming that all 1^+ states seen are $T=2$.

As seen from Tables II and III, the measured strength quoted for the lowest $T=2$ state appears slightly larger than that predicted. One explanation of such a discrepancy is that the model wave functions incorporate too much configuration mixing; consequently, the strength predicted in the T_i+1 channel is quenched too much. The experimental strength extracted above 13 MeV depends strongly on the assumption made about the background, as described in Sec. III. Of the three forms discussed in Sec. III, the one chosen to obtain the quoted experimental numbers yields the largest GT strength; however, the strength of the $T=2$ state would be reduced by about 14% if a polynomial background is chosen for the entire spectrum. Extrapolation of the cross section to $q=0.05$ fm⁻¹ introduces an uncertainty of about 4% in the cross section. The convolution of these two uncertainties and the systematic uncertainty in the cross section of 13% yields a resultant uncertainty in the extracted $B(\text{GT})$ for the state at 13.6 MeV of about 20%. Hence we are left with an apparent discrepancy at the level of two standard deviations between experiment and this component of the shell-model predictions.

In summary, our analysis with shell-model wave functions of the measured excitation-energy spectrum for the $^{26}\text{Mg}(p,n)^{26}\text{Al}$ reaction leads to the following conclusions.

- (1) The strength observed below an excitation energy of 15 MeV is slightly more than half (or 57%) of that predicted.
- (2) Little strength is observed or predicted between 15

citation energy of 13.55 ± 0.06 MeV.

(3) The predicted distribution of strength between the $T=0$, 1, and 2 channels is consistent with the experimental observations, except that the relatively small fraction of strength in the $T=2$ channel is predicted to be too small on an absolute scale. Rigorous isospin assignments are not possible everywhere in the spectrum.

(4) Analysis of the shell-model results indicates that the sensitivity of the predicted strength to configuration mixing increases with increasing isospin; hence, the $T=0$ comparison should be most reliable in terms of extracting a quenching factor, while the $T=2$ results indicate that the shell-model wave functions may incorporate too much configuration mixing.

VI. CONCLUSIONS

The present experiment has yielded a detailed view of the dominant portion of the GT transition strength from ^{26}Mg to ^{26}Al . The experimental spectrum suggests little strength above an excitation energy of 15 MeV; similarly, structure calculations that reproduce the profile of strength distribution over the first 15 MeV of excitation energy predict that little strength remains within the conventional shell-model space above 15 MeV. This ability to survey experimentally the dominant portion of GT strength is the attribute of the (p,n) reaction that makes it an invaluable complement to weak-interaction decays.

The mediator of actual Gamow-Teller beta decay, an operator which transfers both spin and isospin, is particularly simple and restrictive in its action. Hence the values of its matrix elements between nuclear states can be related to sum rules and to specific wave function properties with relative clarity. Thus, systematic deviations between GT beta-decay observations and the analogous predictions of conventional nuclear theory, such as described in Ref. 30, can have fundamental implications about nuclear structure at a more general level; however, the confidence to be attached to such implications is limited by the experimental fact that typical beta decays have small Q values and can sample only the lowest few levels in the daughter system. The dominant spin-transfer nature of the GT process pushes much of the GT strength to an excitation energy characteristic of the spin-orbit splitting,

namely 7–10 MeV; as a consequence, typical matrix elements to states in the first two or three MeV of excitation constitute only a fraction of the total strength.

As mentioned, and as illustrated in Table III, the extraction from experimental GT strengths of a quantitatively accurate estimate of a global quenching factor depends upon analysis of the data with a theoretical model for the mixing of the conventional shell-model configurations. Confidence in the value of the extracted quenching factor for nuclei with significant ground-state correlations rests on confidence in the underlying theoretical model. As long as the range of data sampled is constricted to the low-energy part of a distribution typically centered at 10 MeV, the possibility of significant error exists in the theoretical strengths predicted for the lowest-energy part of such a distribution.

The apparently accurate simulation of GT processes with the medium-energy (p,n) reaction provides a critical resolution of the dilemma posed by the Q -value limitations of ordinary beta decay. Since the entire characteristic profile of the GT strength can be observed with the (p,n) reaction, the validity of the nuclear structure model analysis can be checked in a much more thorough fashion. The residual limitations of the (p,n) reaction as a GT probe (namely the uncertainty in the level of precision for simulating the $\sigma \cdot \tau$ operator, and the problem of separating $L=0$ strength from $L=1$ strength and continuum strength at higher excitation energies) are insignificant relative to the central facts that the (p,n) data (i) match accurately the relative strengths of GT beta transitions, (ii) provide a view of the complete strength distribution, and (iii) together with actual beta decay and systematic theoretical analysis yield convincing detailed evidence for a global quenching of GT strength. The present results for the $^{26}\text{Mg}(p,n)^{26}\text{Al}$ reaction point the way to a new level of precision in the study of GT processes and of nuclear structure models.

ACKNOWLEDGMENTS

This work was supported in part by the National Science Foundation under Grant No. PHY 83-40353, PHY 85-01054, and PHY 83-12245. The authors thank Dr. B. A. Brown for valuable conversations and assistance with some of the theoretical interpretation.

*Present address: University of Maryland, College Park, MD 20742.

† Present address: Drexel University, Philadelphia, PA 19104.

¹H. Toki, Phys. Rev. C **26**, 1256 (1980).

²C. D. Goodman, C. C. Foster, S. D. Bloom, C. Gaarde, J. Larsen, C. A. Goulding, D. J. Horen, J. G. Masterson, J. Rapaport, T. N. Taddeucci, and E. Sargarbaker, Nucl. Phys. A **374**, 241c (1982).

³W. A. Sterrenburg, Sam M. Austin, U. E. P. Berg, and R. DeVito, Phys. Lett. **91B**, 337 (1980).

⁴U. E. P. Berg, Sam M. Austin, R. DeVito, A. I. Galonsky, and W. A. Sterrenburg, Phys. Rev. Lett. **45**, 11 (1980).

⁵N. Anantaraman, S. M. Austin, G. M. Crawley, A. Galonsky,

H. Toki, B. D. Anderson, A. R. Baldwin, B. S. Flanders, C. Lebo, R. Madey, J. W. Watson, C. C. Foster, and A. G. M. van Hees, submitted to Phys. Rev. C.

⁶C. D. Goodman, C. C. Foster, M. B. Greenfield, C. A. Goulding, D. A. Lind, and J. Rapaport, IEEE Trans. Nucl. Sci. **NS-26**, 2248 (1979).

⁷A. R. Baldwin and R. Madey, Nucl. Instrum. Methods **171**, 149 (1980).

⁸R. Madey, J. W. Watson, M. Ahmad, B. D. Anderson, A. R. Baldwin, A. L. Casson, W. Casson, R. A. Cecil, A. Fazely, J. M. Knudson, C. Lebo, W. Pairsuwan, P. J. Pella, J. C. Varga, and T. R. Witten, Nucl. Instrum. Methods **214**, 401 (1983).

⁹A. Fazely, M. Ahmad, B. D. Anderson, A. R. Baldwin, A. M.

- Kalenda, R. J. McCarthy, J. W. Watson, R. Madey, W. Bertozzi, T. N. Buti, J. M. Finn, M. A. Kovash, B. Pugh, and C. C. Foster, *Phys. Rev. C* **25**, 1760 (1982).
- ¹⁰R. A. Cecil, B. D. Anderson, and R. Madey, *Nucl. Instrum. Methods*, **161**, 439 (1979).
- ¹¹B. D. Anderson, J. N. Knudson, R. Madey, and C. C. Foster, *Nucl. Instrum. Methods* **169**, 153 (1980).
- ¹²J. W. Watson, B. D. Anderson, A. R. Baldwin, C. Lebo, B. S. Flanders, W. Pairsuwan, R. Madey, and C. C. Foster, *Nucl. Instrum. Methods* **215**, 413 (1983).
- ¹³J. D. Auria, M. Dombosky, L. Moritz, T. Ruth, G. Sheffer, T. E. Ward, C. C. Foster, J. W. Watson, B. D. Anderson, and J. Rapaport, *Phys. Rev. C* **30**, 1999 (1984).
- ¹⁴J. R. Wu, *Phys. Lett.* **91B**, 169 (1980).
- ¹⁵B. D. Anderson, T. Chittrakarn, A. R. Baldwin, C. Lebo, R. Madey, P. C. Tandy, J. W. Watson, B. A. Brown, and C. C. Foster, *Phys. Rev. C* **31**, 1161 (1985).
- ¹⁶R. Schaeffer and J. Raynal, Program DWBA70 (unpublished); extended version DW81 by J. R. Comfort (unpublished).
- ¹⁷M. A. Franey and W. G. Love, *Phys. Rev. C* **31**, 488 (1985).
- ¹⁸C. Olmer, A. D. Bacher, G. T. Emery, W. P. Jones, D. W. Miller, H. Nann, S. Yen, T. E. Drake, and R. J. Sobie, *Phys. Rev. C* **29**, 361 (1984).
- ¹⁹B. A. Brown, private communication.
- ²⁰H. S. Wilson, R. W. Kavanagh, and F. M. Mann, *Phys. Rev. C* **22**, 1696 (1980).
- ²¹B. A. Brown and B. H. Wildenthal, *Phys. Rev. C* **28**, 2397 (1983). Note that $B(GT)$ defined in this reference differs from the $B(GT)$ defined here by a factor of $(g_A/g_V)^2 = (1.262)^2$.
- ²²D. H. Wilkinson, *Nucl. Phys. A* **377**, 474 (1982).
- ²³S. J. Freedman, private communication.
- ²⁴T. Kajino, H. Toki, and S. M. Austin, *Astrophys. J.* (to be published).
- ²⁵C. Gaarde, J. S. Larsen, M. N. Harakeh, S. Y. van der Werf, M. Igarshi, and A. Muller-Arnke, *Nucl. Phys. A* **334**, 248 (1980).
- ²⁶A. Fazely, B. D. Anderson, M. Ahmad, A. R. Baldwin, A. M. Kalenda, R. J. McCarthy, J. W. Watson, R. Madey, W. Bertozzi, T. N. Buti, J. M. Finn, M. A. Kovash, B. Pugh, and C. C. Foster, *Phys. Rev. C* **25**, 1760 (1982).
- ²⁷B. H. Wildenthal, *Bull. Am. Phys. Soc.* **27**, 725 (1982); *Prog. Part. Nucl. Phys.* **11**, 5 (1984).
- ²⁸B. H. Wildenthal and W. Chung, *The (p,n) Reaction and the Nucleon-Nucleon Interaction*, edited by C. D. Goodman *et al.* (Plenum, New York, 1980), p. 89.
- ²⁹S. D. Bloom, C. D. Goodman, S. M. Grimes, and R. F. Hausman, Jr., *Phys. Lett.* **107B**, 336 (1981).
- ³⁰B. A. Brown and B. H. Wildenthal, *At. Data Nucl. Data Tables* **33**, 347 (1985).
- ³¹P. M. Endt and C. Van der Leun, *Nucl. Phys. A* **310**, 1 (1978).
- ³²A. H. Wapstra and G. Audi, *Nucl. Phys. A* **432**, 1 (1985).
- ³³E. R. Flynn and J. D. Garrett, *Phys. Rev. C* **9**, 210 (1974).
- ³⁴W. L. Bendel, L. W. Fagg, R. A. Tobin, and H. F. Kaiser, *Phys. Rev.* **173**, 1103 (1968).